Optical Trap Assisted Nanoscale Laser Direct-Write Patterning

Paper (N101)

James Joy, Euan McLeod, Craig B. Arnold

Department of Mechanical and Aerospace Engineering and Princeton Institute for Science and Technology of Materials, Princeton University
Princeton, NJ 08544, USA

Abstract

Laser direct-write patterning methods are traditionally limited by the diffraction limit to size scales several hundreds of nanometers at the minimum. In this work, we demonstrate a new method of laser based patterning that overcomes these limitations by taking advantage of near-field enhancement at the surface of dielectric microspheres. Polystyrene microspheres are trapped in CW Bessel beam laser traps above a polyimide surface. A second, pulsed ultraviolet laser gets focused through the bead, and produces nanometer scale features on the substrate. The full width, half maximum of the features generated by this technique is measured and analyzed along with Finite Difference Time Domain simulations to predict the effects of bead size and pulsed laser energy. It is demonstrated that using a 0.76 μm sphere to focus the processing laser results in spots with an average size of 130 nm and a standard deviation of 38 nm, showing that spots with sizes below the diffraction limit can be generated.

Introduction

Advancements in nanotechnology require features smaller than 100 nm with the ability to rapidly prototype arbitrary patterns. A variety of techniques [1-3] are capable of producing such structures, but various experimental limitations continue to encourage the development of new methods. Optical techniques have many benefits such as speed, and ease of use, however, since the Rayleigh diffraction limit sets the minimum possible size of spots at one half of the processing wavelength, optical techniques using ultraviolet processing lasers are often abandoned in favor of techniques involving atomic force microscopy or chemical methods [4]. Such techniques are often much slower, more expensive, and some even require complicated feedback mechanisms throughout the direct write process to control the location of the tip relative to the substrate of interest. Thus, while they have the advantage of creating smaller feature sizes than traditional laser direct-writing techniques, they abandon the speed and ease of use with which optical patterning can be performed [5].

Optical trap assisted nanopatterning seeks to overcome many of the limitations of other optical nanopatterning approaches by offering the ability to produce minimum feature sizes smaller than one half of the processing wavelength, as well as to allow the patterning of surfaces according to a user-defined pattern [6]. Moreover, it seeks to be relatively inexpensive, fast, and have the added benefit of parallelization. In this technique, a polystyrene microsphere is used as a near-field focusing objective to concentrate the radiation from the processing laser onto a small area on the surface of a substrate.

More specifically, we employ a Bessel beam optical trap [7] to position the microspheres near the surface. The diffractionless behavior of this type of optical trap enables confinement in the x-y directions while maintaining a constant scattering force in the z-direction over large distances. As the dielectric sphere approaches the substrate, it encounters a repulsion force that serves to balance the optical scattering force. The end result is that the bead will attain an equilibrium position that is independent of large scale features on the surface. This self-positioning effect enables the bead to maintain a constant distance from the surface without the need for additional or active feedback. Nanopatterning is accomplished with a second, pulsed ultraviolet, laser that is focused by the microsphere on the substrate below.

In this paper, we examine the effects of optical trap-assisted near-field nanopatterning on the model substrate system of polyimide. The ablation threshold of polyimide films has been theoretically and experimentally studied for varying pulse lengths and pulse fluences at different wavelengths and therefore it is possible to not only experimentally study the

capabilities of our method, but also to theoretically predict the spot sizes that will result. To this end, we use finite difference time domain simulations for the optical field.

Methods

Sample polyimide films are prepared by spin coating polyimide (HD MicroSystems, PI 2525) onto glass cover slips at 500 rpm for 10 seconds, followed by 8000 rpm for 40 seconds. The coverslips are then baked at 150°C for 30 minutes, and subsequently at 350°C for another 30 minutes. This process produces films 3 µm thick.

Commercially available polystyrene microsphere solutions (Bangs Labs 0.46 µm and 0.76 µm, no. PS03N; Ted Pella 1.00 µm no. 610-38; Polysciences 3.0 µm no. 17134) are diluted until the suspensions are dilute enough to prevent more than one sphere from entering into the trapping region during the experiment. Between 1 and 5 µL of the desired solution is pipetted onto the polyimide surface. A square region is cut into a piece of double-sided tape (3M, no. 9589, 230 µm thick), and this is used as a gasket to seal another glass coverslip on top of the polyimide surface providing a sealed chamber approximately 1 cm x 1 cm x 230 µm filled with the bead suspension. This assembly is then mounted onto a piezoelectric xyz stage (ThorLabs, MAX301) that can be controlled either manually or with a piezo controller.

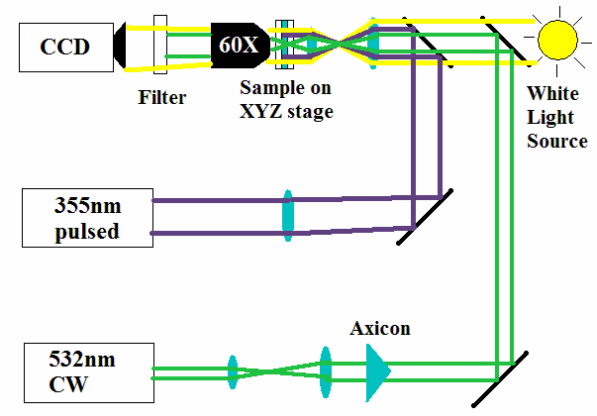

Figure 1: Experimental Setup

The trapping laser (532 nm, CW) is first expanded by a factor of 2 using a telescope, and then passes through a 178 degree axicon lens to produce the Bessel beam. An expanded beam is required so that the resulting Bessel beam has a large enough region over which the beam is non-diffracting. The Bessel beam is then reduced by another telescope, setting the size of the trap to be commensurate with the bead size. The typical power in the central lobe of the Bessel beam is 0.1 - 1 mW.

The UV processing laser (Coherent AVIA, 355 nm pulsed 15-ns) is first sent through a converging lens with a long focal length (500 mm) before being put through only the second telescope described above. Because the beam is not precisely collimated as it enters the telescope, it is slightly converging as it exits and propagates onto the stage. This provides more control over the beam width that is irradiated onto the stage.

This direct-write process is observed with a 50x microscope objective and a CCD camera (Cohu 2622) with an IR filter. Before patterning begins, the user moves the stage manually until a bead is found. The trapping laser is then turned on to trap the bead. Using a predefined set of instructions, a piezo controller connected to the computer moves the stage under the bead in the desired pattern. At each point in the pattern, the stage stops, and a shot is fired from the UV processing laser. If continuous features are required the processing laser can fire overlapping shots between successive points in the pattern.

Patterns are analyzed using scanning electron microscopy and atomic force microscopy. The height of spots are profiled, and a circle is fit to the region at which the height is at half of its maximum. The diameter of this circle is taken to be the FWHM for that spot.

Theoretical models are used as a baseline to predict the capabilities of our technique. FDTD simulations of Maxwell's equations based on the Yee algorithm are generated for the system [8]. The region over which the simulation is generated is a rectangular prism encompassing the sphere, the polyimide surface, as well as some 'depth' of the polyimide. The sphere-surface spacing was taken to be 50 nm based on existing knowledge of the surface interactions [9] and the boundary condition directly above the sphere and the polyimide emits uniform plane waves, as this closely approximates the Gaussian pulse on the order of the diameter of the microsphere. The other boundaries are all taken to absorb the incident radiation to simulate the light travelling off to infinity [10]. The feature size is then calculated to be the region on the surface for which the impinging laser energy density is above the threshold fluence. For this calculation, a modification threshold fluence of polyimide at 355 nm radiation is estimated to be 48 mJ cm^{-2} based on models developed by Piglmayer et al. [11].

Results

It has been established that UV laser radiation not only changes the topology of a polyimide film [12], but can also change the chemical properties of the film's surface [13]. In response, polyimide film will form either a bump when irradiated with a pulsed laser of fluence just below the ablation threshold, it will begin to form a bump with a hole as the fluence of the incident radiation is increased, and ultimately at higher fluences will form a traditional ablation pit. These properties can be tailored to produce a desired topology on the substrate being patterned. For the purposes of this paper, we do not distinguish between these different topological features.

Spot sizes are measured for processing laser fluences of 5, 7, 12, 13, and 35 mJ/cm^{-2} and presented in figure 2. Higher laser fluences than this range approach the ablation threshold of polyimide without near-field enhancement, in which case, the unfocused laser beam would begin to affect the surface. Thus, these fluences will produce spot sizes on the order of the width of the Gaussian pulse, and are not of interest to the experiment. In general larger laser fluences, as well as larger focusing beads, cause larger features on the polyimide surface as shown in the figure for both the experimental measurements and theoretical calculations. For instance, 1 µm diameter bead can produce features with mean size of 150 nm, 400 nm, or 600 nm depending on the fluence used in this experiment. As the bead diameter is decreased, the feature size eventually levels off at approximately 100 nm.

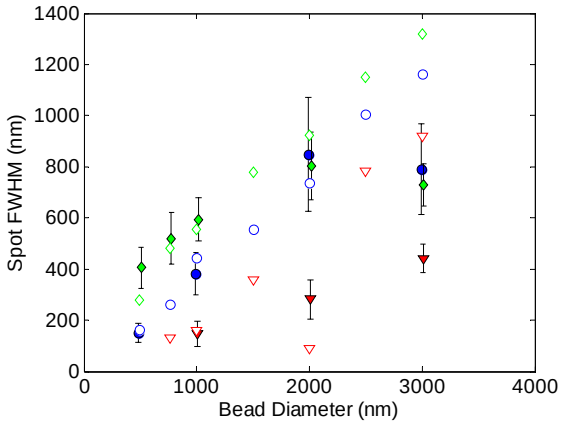

Figure 2: Spot FWHM of various bead sizes at varying fluences. The green diamonds have a fluence of 35 mJ cm^{-2}, the blue circles have a fluence of 12 mJ cm^{-2} and the red triangles have a fluence of 5 mJ cm^{-2}. Experimental data is represented by the filled shapes, while FDTD calculations are represented by the unfilled shapes.

The reason for the leveling as the microsphere size decreases is related to the decrease in near-field intensity enhancement as a function of sphere size. Figure 3 shows the calculated intensity enhancement at a plane 50 nm below the sphere with varying sphere diameters. As we can see, these do not follow an elementary functional form with the model, suggesting the greatest intensity enhancement with this bead-surface separation distance occurs for spheres with a diameter of approximately 1 µm. Large spheres have back focal distances much greater than the 50 nm spacing, and therefore the intensity enhancement at the surface does not continue to increase with sphere size. The non-monotonicity of the intensity enhancement in this region is due to spherical aberrations in the focused field. As the intensity enhancement decreases, the ability to produce a sharp feature decreases since one requires higher fluences to obtain local energy densities above the threshold values. Given these effects, there exists a balance between the feature sizes that can be fabricated with small spheres and the decrease in intensity enhancement. In the current experiment, it is found that 0.76 µm polystyrene spheres give good intensity enhancement: about 15x the incident laser fluence while providing small features sizes approximately 100 nm in diameter.

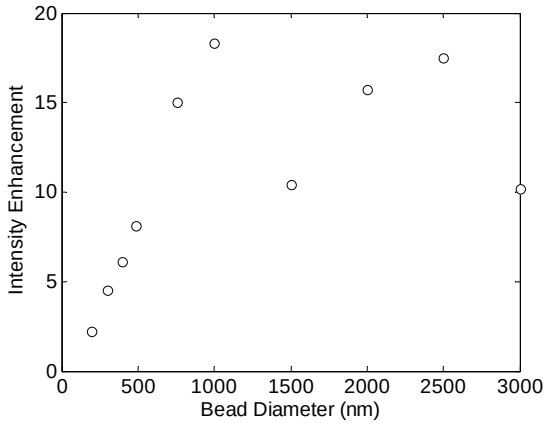

Figure 3: Figure 3: Intensity enhancement predictions for a plane 50 nm below the bead. Notice that the peak enhancement in this plane is predicted for spheres with diameters of about 1 µm.

In order to produce reliable patterns, it is necessary to be able to accurately position the microbead with high resolution. This also sets an effective limit on the particle size. As the particle decreases in size, Brownian motion increases for a given trapping laser intensity, thereby making it more difficult to accurately position the bead. Once again, particle sizes of 0.76 µm provide a reasonable compromise allowing

accurate placement to about 40 nm depending on the trapping laser intensity.

Theoretical calculations of the accuracy of the positioning of the microspheres in the Bessel beam trap can provide a more quantitative measure of the accuracy as a function of the particle size [6]. The main contribution to particle motion in x-y can be attributed to Brownian motion. This random fluctuation is countered by the potential landscape provided by the optical trap. Or in other words, the stronger the trap, the greater the optical force on the particle and the less motion that will occur due to Brownian motion. Thus an assessment of the accuracy of the positioning of the particle can be made by calculating the expectation value of the sphere's position.

The probability of finding a particle in a region between r and $r + dr$ in cylindrical coordinates is given by,

$$P(r)dr = 2\pi r A \exp\left(-\frac{U(r)}{kT}\right)dr, \qquad (1)$$

where A is a normalization constant, $U(r)$ is the potential energy of the radiation field, k is Boltzmann's constant, and T is the temperature. The potential energy of the particles can be expressed as [6, 14].

$$U(r) = -\frac{2\pi n_b a^3}{c}\left(\frac{\left(n_p / n_b\right)^2 - 1}{\left(n_p / n_b\right)^2 + 2}\right) I(r), \qquad (2)$$

where n_b is the refractive index of the surrounding medium, n_p is the refractive index of the particle, a is the radius of the particle, c is the speed of light, and $I(r)$ is the intensity of the trapping laser beam. Finally, The intensity can be expressed as,

$$I(r) = \frac{P_0}{0.85a^2} J_0{}^2\left(\frac{2.40r}{a}\right), \qquad (3)$$

with, P_0 is the power in the central lobe of the Bessel beam, a is the particle radius, and 2.40 is first zero of $J_0{}^2(x)$.

Combining these equations enables one to calculate the mean positional error of a microsphere by integrating equation 1. For instance, using 1 mW of trapping power through 0.76 μm polystyrene particle will yield a mean positional uncertainty of approximately 10 nm. Although the uncertainty scales inversely with the trapping laser power, as the laser power is increased, the sphere-surface distance can change, leading to additional effects on the nanoscale features produced.

Similar calculations can be performed for the expectation value of the distance between the microspheres and the surface of the substrate when the sphere is trapped. In this case, there is a balance between the optical scattering force and the sphere-surface repulsion leading to a potential well. Increasing the trapping power not only reduces the distance between the sphere and the surface, but it also lowers the standard deviation of this distance [6]. Thus, higher trapping powers result in spheres relatively close to the surface with very little variation in height. Moreover, since this spacing is due to only the radiation pressure from the trapping laser and the electrostatic repulsion from the surface, the bead should track the surface as it encounters different topology—the same expectation values and standard deviations in sphere height should be measured for the same surface materials and trapping powers regardless of the shape of the surface.

One of the important benefits of our approach as discussed above is that the trapping laser power can help to reduce the positional uncertainty of the sphere. However, one additional point to keep in mind is that since the bead is suspended in a liquid, we have a highly damped system. Therefore, any additional fluctuations such as those from system or building vibrations, or deflections due to the pulsed processing laser, will be damped away quickly. In fact, all of the data presented in this paper are collected in an optical set-up without any vibration isolation on a table rigidly mounted to the floor.

By overlapping subsequent shots, continuous features can be produced using this technique. Figure 4 shows such a structure. In this SEM image, one can see lines approximately 120 nm wide produced using a 0.76 μm bead with a processing laser of 15 mJ/cm^2. These lines can be made into either ridges or valleys by varying the fluence of the incident radiation from the processing laser: ridges would be patterned by using a processing fluence that is located between the modification threshold (~48 mJ/cm^2) and the ablation threshold (~65 mJ/cm^2), while valleys can be patterned by using a processing fluence near the ablation threshold. Once again, since the particle is self-positioned above the surface, once a feature is produced, the bead will still maintain the proper distance from the surface enabling the overlapping spots to produce continuous features.

Finally, figure 5 demonstrates a more complex pattern that can be fabricated through this method. In this SEM micrograph we see a "P" that is less than 1 μm tall, with a line width of approximately 200 nm. One can clearly see the high resolution of the patterning method. In this case, as in figure 4, the dominant feature is a ridge with the desired pattern.

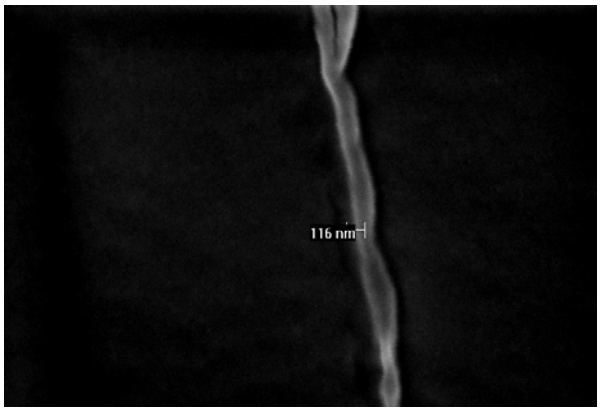

Figure 4: SEM of a narrow line (116 nm). Spacing between the shots was 50 nm.

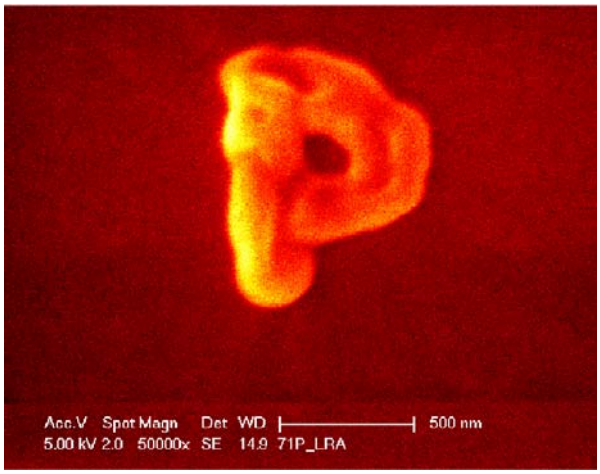

Figure 5 SEM of the letter 'P' generated with shot spacing of 5 nm. This demonstrates the ability of optical trap assisted nanopatterning to produce very small arbitrary patters (this shape is about 500 nm wide by 1000 nm tall).

Conclusion

We have introduced a new method of producing nanoscale features on a surface using a laser based direct write process based on optical trap assisted nanopatterning. The near-field effects at the surface of a microsphere are exploited using a Bessel beam optical trap to manipulate the bead along the surface. Such a trap enables the bead to find an equilibrium position above the surface that is independent of large scale features, thereby enabling us to overcome one of the main challenges with other probe based direct-write nanopatterning methods. Its ability to create arbitrary patterns also allows it to be used in a wide variety of applications, as it can be used to directly write patterns and arrays onto surfaces.

Feature sizes approximately 100 nm have been produced with individual spots and continuous features. In general, the smaller the bead size, the smaller the features that can be produced. However, limitations due to Brownian motion and near-field intensification limit the minimum bead size to approximately 0.5 to 1.0 μm, for polystyrene beads. In the special case of the polyimide model system presented here, both ridges and valley can be produced with high resolution.

References

[1] Kawata, S., Sun, H.-B., Tanaka, T. & Takada, K. (2001) Finer features for functional microdevices, Nature 412, 697-698.

[2] Hwang, D.J., Chimmalgi, A. & Grigoropoulos, C.P. (2006) Ablation of thin metal films by short-pulsed lasers coupled through near-field scanning optical microscopy probes, J. Appl. Phys. 99, 044905.

[3] Chimmalgi, A., Grigoropoulos, C.P. & Komvopoulos, K. (2005) Surface nanostructuring by nano-femtosectond laser-assisted scanning force microscopy, J. Appl. Phys. 97, 104319.

[4] Chen, Y.J., Hsu, J.H. & Lin, H.N. (2005) Fabrication of metal nanowires by atomic force microscopy nanoscratching and lift-off process, Nanotechnology 16, 1112-1115.

[5] Arnold, C.B., Serra, P. & Pique, A. (2007) Laser direct write of complex materials, MRS Bull. 32, 23-31.

[6] McLeod, E. & Arnold, C.B. (2008) Subwavelength direct-write nanopatterning using optically trapped microspheres, Nature Nanotech. 3, 413-417.

[7] McGloin, D. & Dholakia, K. (2005) Bessel beams: Diffraction in a new light, Contemp. Phys. 46, 15-28.

[8] Yee, K.S. (1966) Numerical solution of initial boundary value problems involving maxwell's equations in isotropic media, IEEE T. Antenn. Propag. AP-14, 302-307.

[9] Verwey, E.J.W. & Overbeek, J.T.G. (1948) Theory of the stability of lyophobic colloids, Elsevier Publishing Company, Inc.,

[10] Mur, G. (1981) Absorbing boundary conditions for the finite-difference approximation of the time-domain electromagnetic-field equations, IEEE T. Electromagn. C. EMC-23, 377-382.

[11] Piglmayer, K., Arenholz, E., Ortwein, C., Arnold, N. & Bauerle, D. (1998) Single-pulse ultraviolet laser-induced surface modification and ablation of polyimide, Appl. Phys. Lett. 73, 847-849.

[12] Himmelbauer, M., Arenholz, E., Bauerle, D. & Schilcher, K. (1996) Uv-laser-induced surface topology changes in polyimide, Appl. Phys. A 63, 337-339.

[13] Lu, Q.-H., Li, M., Yin, J., Zhu, Z.-K. & Wang, Z.-G. (2001) Polyimide surface modification by pulsed ultraviolet laser irradiation with low fluence, J. Appl. Polym. Sci. 82, 2739-2743.

[14] Harada, Y. & Asakura, T. (1996) Radiation forces on a dielectric sphere in the rayleigh scattering regime, Opt. Commun. 124, 529-541.